Nuclear Engineering and Technology 49 (2017) 224–233

Available online at ScienceDirect

Nuclear Engineering and Technology

journal homepage: www.elsevier.com/locate/net

Original Article

Experimental Study on the Shrinkage Properties and Cracking Potential of High Strength Concrete Containing Industrial By-Products for Nuclear Power Plant Concrete

*Baek-Joong Kim and Chongku Yi**

School of Civil, Environmental and Architectural Engineering, Korea University, 145 Anam-ro, Seongbuk-gu, Seoul 02841, Republic of Korea

ARTICLE INFO

Article history:
Received 14 September 2015
Received in revised form
2 May 2016
Accepted 8 July 2016
Available online 12 August 2016

Keywords:
Nuclear power plant
High strength concrete
Industrial by-product shrinkage
Cracking potential

ABSTRACT

In Korea, attempts have been made to develop high strength concrete for the safety and design life improvement of nuclear power plants. In this study, the cracking potentials of nuclear power plant-high strength concretes (NPP-HSCs) containing industrial by-products with W/B 0.34 and W/B 0.28, which are being reviewed for their application in the construction of containment structures, were evaluated through autogenous shrinkage, unrestrained drying shrinkage, and restrained drying shrinkage experiments. The cracking potentials of the NPP-HSCs with W/B 0.34 and W/B 0.28 were in the order of 0.34FA25 > 0.34FA25BFS25 > 0.34BFS50 > 0.34BFS65SF5 and 0.28FA25SF5 >> 0.28BFS65SF5 > 0.28BFS45SF5 > 0.28 FA20BFS25SF5, respectively. The cracking potentials of the seven mix proportions excluding 0.28FA25SF5 were lower than that of the existing nuclear power plant concrete; thus, the durability of a nuclear power plant against shrinkage cracking could be improved by applying the seven mix proportions with low cracking potentials.

1. Introduction

Industrial by-products such as fly ash [1,2], blast furnace slag [3], and silica fume [4] have been used as supplementary cementing materials in concrete. Fly ash is effective for improving the workability of fresh concrete and for improving the long-term strength/durability and reducing the shrinkage of hardened concrete [5]. Blast furnace slag is effective for reducing the hydration heat of concrete, suppressing alkali-aggregate reactions, and improving water tightness, long-term strength, and resistance to salt damage [6]. With the improved performance of concrete, industrial by-products have been widely applied to civilian structures and their replacement ratios have increased [7].

In contrast to concrete used for civilian structures, the use of industrial by-products in Korea has been relatively limited in nuclear power plant concrete (NPP-C). In 2004, a study by Korea Hydro and Nuclear Power (Seoul, Korea) assessed the application of industrial by-products as supplementary cementing materials of NPP-C with a compressive strength of 5,000–6,000 psi at 28 days [8]. However, among the industrial by-products, only fly ash was used as the supplementary

* *Corresponding author.*
E-mail address: chongku@korea.ac.kr (C. Yi).
http://dx.doi.org/10.1016/j.net.2016.07.007

cementing material of NPP-C for the construction of NPPs in Korea until 2010.

Since 2010, there have been renewed attempts to apply a variety of industrial by-products to develop NPP-C that has a target compressive strength of 6,000 psi at 91 days [9], and thereby meet the required compressive strength for concrete in an exposed condition, as Code ACI 349-06 by the American Concrete Institute (ACI) (Farmington Hills, MI, USA). For the construction of the Singori-3 and -4 nuclear power plants, which were completed in Korea in 2014, the cracking of the NPP-C was suppressed by delaying the initial strength development of the NPP-C by substituting 20% of the cement with fly ash. For the Bakara NPPs in the United Arab Emirates, the durability of the NPP-C was increased by using blast furnace slag and silica fume as the supplementary cementing materials. In addition, with increased societal interest in the safety of NPPs after the Fukushima Daiichi nuclear disaster in 2011, Korea Hydro and Nuclear Power has initiated a new study to develop a NPP high strength concrete (NPP-HSC) with a compressive strength of more than 8,000 psi for an improved design life and safety of nuclear power plants and to secure the performance of the concrete needed for the construction of nuclear power plants in foreign countries.

The typical mix design of high strength concrete requires a large amount of cement to be mixed with a small amount of water. Thus, the risk of concrete cracking increases because of the hydration heat and autogenous shrinkage in the early age [10]. The durability of the structure may also diminish because of harmful agents that ingress through the formed cracks. However, in the construction package specification currently applied to NPP-C, only the allowable range of the drying shrinkage strain (ε_{drying}) is presented, and content relevant to the restraint condition, which affect shrinkage cracking, and the autogenous shrinkage strain (ε_{auto}) are not included. Therefore, in this study, the cracking potentials of NPP-HSCs containing industrial by-products were evaluated with consideration of the autogenous/drying shrinkage characteristics and restraint conditions. The results may provide valuable data for the further development and implementation of high strength concrete for nuclear power plants.

2. Materials and methods

2.1. Materials

Type 1 Portland cement with a density of 3.11 g/cm^3 was the basic binder. Table 1 shows the chemical composition and

Table 1 – Chemical composition of the cement (by wt.%).

CaO	SiO_2	Al_2O_3	MgO	Fe_2O_3	SO_3
58.6	22.1	6.4	4.1	3.5	2.6
K_2O	TiO_2	P_2O_5	Na_2O	Ig.loss	
1.8	0.3	0.3	0.2	0.2	

Al_2O_3, aluminum oxide; CaO, calcium oxide; Fe_2O_3, iron (III) oxide; K_2O, potassium oxide; MgO, magnesium oxide; Na_2O, sodium oxide; P_2O_5, diphosphorus pentoxide; SiO_2, silicon dioxide; SO_3, sulfur trioxide; TiO_2, titanium dioxide.

Table 2 – Mineral composition of the cement (by wt.%).

C_3S	C_2S	C_3A	C_4AF	Gypsum
51.87	19.42	4.84	10.27	3.90

C_3S, tricalcium silicate; C_2S, dicalcium silicate; C_3A, tricalcium aluminate; C_4AF, tetracalcium alumino ferrite.

Table 3 – Density of the supplementary cementing materials (g/cm^3).

Fly ash	Blast furnace slag	Silica fume
2.21	2.90	2.20

Table 2 shows the mineral composition of the cement used in this study.

Fly ash, blast furnace slag, and silica fume were the supplementary cementing materials of the cement. Table 3 shows the density of the supplementary cementing materials and Table 4 shows their chemical composition.

The fine aggregate was sand with a density of 2.6 g/cm^3 and a water absorption ratio of 2.5%. The coarse aggregate was gravel with a density of 2.62 g/cm^3 and a maximum size of 20 mm. The chemical admixture was a polycarboxylate type high-performance water-reducing agent with a solid content of 25.5% and a density of 1.06 g/cm^3.

2.2. Mix proportion of concrete

In this experiment, nine concrete mix proportions with a water-to-binder ratio (W/B) of 0.40, 0.34 and 0.28 were prepared: one concrete mix proportion (W/B 0.40), which had been applied to the Singori NPPs completed in 2014 among existing NPP-Cs, and eight mix proportions (W/B 0.34 and W/B 0.28) of NPP-HSCs under review for application. The mix proportions of NPP-HSCs were designed so that the specific compressive strength (i.e., 55.16 MPa for W/B 0.34 and 68.95 MPa for W/B 0.28) could be obtained before the curing age of 91 days. In addition, for the reduced hydration heat and autogenous shrinkage in NPP-HSCs, the mix proportions of NPP-HSCs had higher replacement ratios of supplementary cementing material for Portland cement than that for NPP-Cs. The details of the mix proportions of the concretes in this study are in Table 5.

2.3. The manufacture of the specimens and the experimental method

2.3.1. Slump, air content, and compressive strength of concrete

The workability (i.e., slump or slump flow) and air content of fresh concrete were measured in accordance with American Standard Test Methods (ASTM) Standards C143/C143M and C173/C173M-14, respectively [20,21]. The cylinder specimen (φ100 × 200 mm) was cast in plastic molds and stored at a constant temperature (21.5 ± 2°C) and humidity (50%) chamber. The mold was removed after 24 hours. The cylinder specimen was then water-cured in a constant temperature water tank at 20 ± 1°C. The compressive strength was

Table 4 – Chemical composition of the supplementary cementing materials (by wt.%).

Type	CaO	SiO_2	Al_2O_3	MgO	Fe_2O_3	SO_3	Na_2O
Fly ash	8.48	39.69	19.15	2.67	18.57	0.45	0.47
Blast furnace slag	37.59	35.01	16.18	5.96	0.37	2.91	0.17
Silica fume	–	93.90	–	–	–	–	–

Al_2O_3, aluminum oxide; CaO, calcium oxide; Fe_2O_3, iron (III) oxide; MgO, magnesium oxide; Na_2O, sodium oxide; SO_3, sulfur trioxide.

measured at 3 days, 7 days, 14 days, 28 days, and 56 days, based on ASTM Standard C39/C39M-15a [22].

2.3.2. Shrinkage of concrete

2.3.2.1. *Unrestrained shrinkage of concrete.* To measure autogenous shrinkage, a specimen (75 mm × 75 mm × 400 mm) was prepared (Fig. 1). An acrylic mold was used to prevent moisture loss from the specimen. A polytetrafluoroethylene sheet was used to eliminate adhesion or friction between the acrylic mold and the concrete. A strain gauge for measuring ε_{auto} was installed at the center of the specimen, and a thermocouple was installed to measure the temperature change within the specimen due to the hydration heat. The measured temperature was used to correct the effect of hydration heat on ε_{auto} in accordance with KS F 2586 [23].

To measure the drying shrinkage, a specimen 75 mm × 75 mm × 400 mm was used (Fig. 2). Based on ASTM Standard C 596, the specimen was manufactured using a steel mold [24]. The mold was then sealed with a vinyl sheet to prevent moisture loss. The mold of the specimen was removed at the curing age of 24 hours. Strain gauges for measuring ε_{drying} were installed on two flat side faces of the specimen at the center.

2.3.2.2. *Restrained shrinkage of concrete.* For a ring specimen, suggested by ASTM Standard C 1581-04 and American Association of State Highway and Transportation Officials (AASHTO) PP 34-99, it is easy to measure the cracking occurrence time and restraint stress for concrete due to shrinkage [25]. The ASTM Standard C 1581-04 limits the maximum size of the coarse aggregate of concrete to 13 mm; thus, based on the guidelines of AASHTO PP 34-99, the ring specimen (Fig. 3) used in this study was manufactured at the maximum size (20 mm) of coarse aggregate.

To measure the strain of the inner steel ring (ε_s) of the ring specimen, four strain gauges were installed at equal intervals on the inner sides of the inner steel ring. After placing the concrete, the mold was sealed with a vinyl sheet to prevent moisture loss from the ring specimen. The outer steel ring of the ring specimen was removed at 24 hours, and the upper surface of the concrete was coated with paraffin so that moisture could evaporate only through the outer circumferential sides of the concrete.

2.3.2.3. *Curing and strain measurement.* All specimens used for the measurement of shrinkage were cured in a constant temperature and humidity room at a temperature of 21.5 ± 2°C and a relative humidity of 50% for the entire curing age. The strain gauge installed in the specimen was connected to a data logger, and ε_{auto}, ε_{drying}, and ε_s were measured at 10-minute intervals.

3. Analysis of unrestrained and restrained shrinkage

3.1. Normalization of ε_{auto} and ε_{drying}

To compare ε_{auto} and ε_{drying} of NPP-HSC with those of NPP-C, these strain values were normalized using Eqs. (1) and (2), respectively.

$$NAS(t) = \frac{\varepsilon_{auto}(t)\ of\ NPP-HSC}{\varepsilon_{auto}(t)\ of\ NPP-C} \quad (1)$$

$$NDS(t) = \frac{\varepsilon_{drying}(t)\ of\ NPP-HSC}{\varepsilon_{drying}(t)\ of\ NPP-C} \quad (2)$$

in which NAS is the normalized autogenous shrinkage (με/με), NAS is the normalized drying shrinkage (με/με), and t is the curing time.

3.2. Cracking of the restrained shrinkage specimen

The cracking potential of the ring specimen was evaluated by the net time-to-cracking (t_{cr}) and stress rate (S). The variable t_{cr} is the time from the removal of the outer steel ring to the occurrence of cracking, and S is calculated using Eq. (3) [11, 12].

$$S = \frac{|\alpha|}{2\sqrt{t_{cr}}} \frac{r_{ic} \cdot t_s}{r_{is} \cdot t_c} \cdot E_{st} \quad (3)$$

in which r_{ic} is the inner radius of the concrete (mm), t_c is the concrete thickness (mm), r_{is} is the inner radius of the inner steel ring (mm), t_s is the inner steel ring thickness (mm), E_{st} is the elastic modulus of the steel ring (GPa), and α is the value of the strain rate factor [(m/m)/$d^{1/2}$].

The variable α is calculated through linear regression analysis by using Eq. (4).

$$\varepsilon_{net} = \alpha\sqrt{t} + k \quad (4)$$

in which ε_{net} is the net strain (m/m), t is the elapsed time (days), and k is the regression constant.

4. Test results and discussion

4.1. Air content, workability, and compressive strength of concrete

Table 6 shows the air content and workability (i.e., slump or slump flow) of the fresh concretes. The air content of the NPP-HSCs was 3.6–4.8%. The slump of the NPP-HSCs with W/B 0.34 was 180–200 mm, and the slump flows of NPP-HSCs with W/B 0.28 was 500–590 mm. The air content and the workability

Table 5 – Mix Proportions of the concretes used in this study.[a]

Mix [b]		$f_{ck(91\ days)}$ (MPa)	Slump or slump flow (mm)	Air content (%)	W/B	S/a (%)	Unit weight (kg/m³)						
							Water	Binder				Aggregate	
								C	FA	BFS	SF	S	G
NPP-C	0.40FA20	41.36	>180 (slump)	3~5	0.40	44	162	324	81	–	–	747	963
NPP-HSC	0.34FA25	55.16			0.34		155	342	114	–	–	732	942
	0.34FA25BFS25						155	228	114	114	–	730	936
	0.34BFS50						155	228	–	228	–	742	956
	0.34BFS65SF5						155	138	–	296	23	738	947
	0.28FA25SF5	68.95	>500 (slump flow)		0.28		155	388	138	–	28	707	885
	0.28FA20BFS25SF5						155	277	111	138	28	707	885
	0.28BFS45SF5						155	277	–	249	28	720	904
	0.28BFS65SF5						155	166	–	360	28	718	899

BFS, blast furnace slag; C, cement; FA, fly ash; G, gravel; NPP-C, nuclear power plant concrete; NPP-HSC, nuclear power plant high strength concrete; S, sand; SF, silica fume.

[a] The variable $f_{ck(91\ days)}$ is the specific compressive strength at 91 days, W/B is the water-to-binder ratio, and S/a is the fine aggregate modulus in which "a" is the total weight of sand and gravel.

[b] Mix notation includes two parts. The first part is used to identify the W/B ratio by weight and the second part is used to identify the supplementary cementing material-to-binder ratio by weight (for example, 0.40FA20 is a mix having a W/B ratio of 0.40 and FA/B of 20 %).

satisfied the planned mix proportion standards. Fig. 4 shows the compressive strength of the NPP-HSCs measured at 3 days, 7 days, 14 days, 28 days, and 56 days. As mentioned in Section 2.2, the compressive strength of the NPP-HSCs was designed so that the design standard strength was obtained before 91 days, and the measurement of the compressive strengths showed that all mix proportions satisfied the design standard strength at 56 days.

4.2. *Autogenous shrinkage of concrete*

Fig. 5 shows the internal temperature of the specimen and the temperature of the constant temperature and humidity room.

The internal temperatures of the specimens manufactured using the NPP-HSCs increased after the mixing process, and the internal temperatures reached their maximum values at 14–27 hours. After 48 hours, the internal temperature of the specimens was the same as the room temperature. Fig. 6 shows the maximum value of the temperature difference (ΔT_{max}) between the internal temperature of the specimen and the room temperature and $t_{\Delta T_{max}}$, the time of the occurrence of ΔT_{max}.

The ΔT_{max} of NPP-HSCs containing blast furnace slag were lower than that of the NPP-C because of the decrease in the hydration heat [13]. However, ΔT_{max} of the NPP-HSCs containing fly ash were higher than that of NPP-C. In particular, the ΔT_{max} of 0.28FA25SF5 (5.35°C) increased by 39.6%, compared to that of the NPP-C (3.83°C), because of the increase in the unit weight of the binder and the increase in the hydration heat from the mixing of silica fume [14]. Thus, the initial cracking potential due to the hydration heat should be considered when the NPP-HSCs containing fly ash are applied to a NPP.

Fig. 7 shows the ε_{auto} of the NPP-HSC specimen and Fig. 8 shows the NAS.

The ε_{auto} of the NPP-C at 91 days was 55.8 με, and the ε_{auto} of the specimens with a W/B of 0.34 at 91 days were as follows (listed in decreasing order): 0.34BFS50 (163.4 με) > 0.34BFS65SF5 (132.0 με) > 0.34FA25 (79.9 με) > 0.34 FA25BFS25 (45.5 με).

The NAS of 0.34BFS50 was > 1 during the entire curing age, and the maximum value (4.76) appeared at 9 days. The NAS of 0.34BFS50 at 91 days was 2.93, which was the largest value among the NASs of the specimens with W/B 0.34 because of the pore filling effect of blast furnace slag, the particles of which are small and angular [15]. However, the NAS of 0.34BFS65SF5 at 91 days was 2.37, which decreased by 19.5%, compared to that of 0.34BFS50. It may be that the ε_{auto} of concretes containing a large amount of blast furnace slag decreased because of the slow hydration reaction of blast furnace slag and the increasing amount of moisture adsorbed onto the unreacted blast furnace slag [16].

The NAS of 0.34FA25 was < 1 for the first 8 days. This level of autogenous shrinkage of 0.34FA25 at the early curing age can be attributed to the reduced unit weight of cement, which

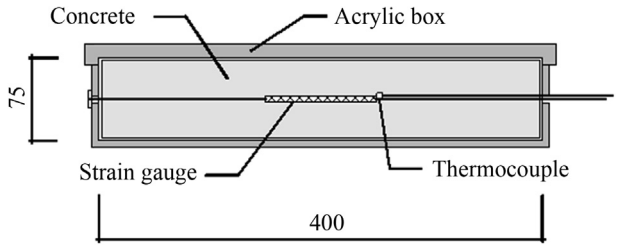

Fig. 1 – Measurement of the autogenous shrinkage in the concrete specimen.

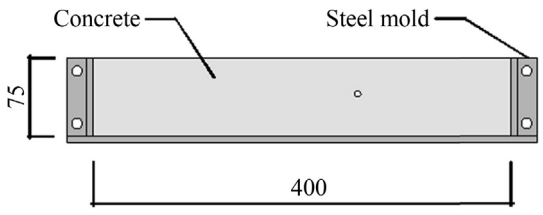

Fig. 2 – Measurement of the drying shrinkage in the concrete specimen.

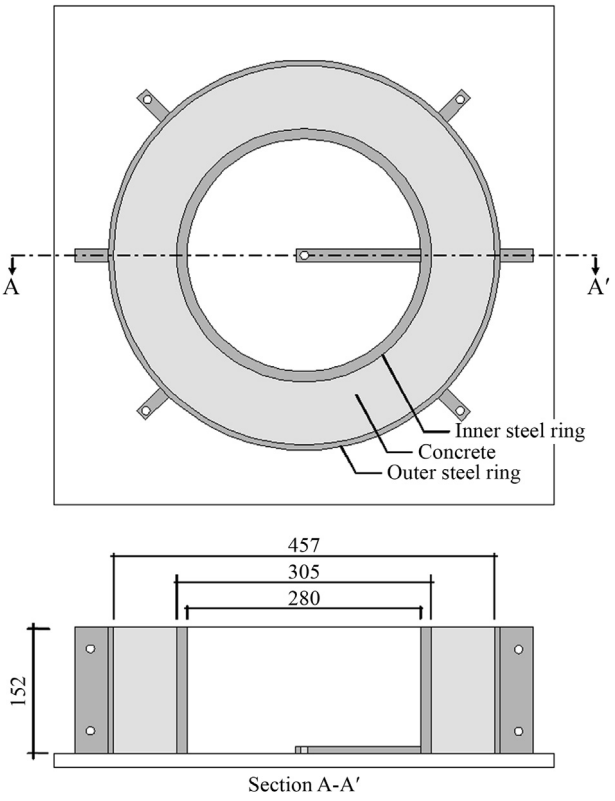

Fig. 3 – Measurement of the restrained drying shrinkage in the concrete specimen.

reduces the amount of calcium hydroxide [$Ca(OH)_2$] needed for the pozzolanic reaction of fly ash [7]. However, the NAS of 0.34FA25 increased steadily until 28 days, and it remained between 1.38 and 1.57 for 28–91 days. It appears that the ε_{auto} of 0.34FA25 was larger than that of the NPP-C because of the increase in the unit weight of the binder within the concrete [17].

The NAS of 0.34FA25BFS25 was < 1 until the curing age of 3 days, and the maximum value (1.79) appeared at 7 days. The NAS at 91 days was 0.82, which was the smallest value among the NASs of the specimens with W/B 0.34. This finding is because of the complex effect of the decrease in the hydration reaction of cement because of the mixing of a large amount of supplementary cementing materials, the decrease in the pozzolanic reaction of fly ash, and the moisture adsorbed onto blast furnace slag.

The ε_{auto} of specimens with W/B 0.28 at 91 days were as follows (listed in decreasing order): 0.28BFS65SF5 (180.5 με) > 0.28BFS45SF5 (164.0 με) > 0.28FA25SF5 (163.0 με) > 0.28FA20BFS25SF5 (62.5 με). The ε_{auto} is generally larger in specimens with W/B 0.28 than in specimens with W/B 0.34. This finding is consistent with the result of a previous study [17], which reported that concrete with a low W/B has a high suction pressure because of small internal pores, and a high suction pressure increases the autogenous shrinkage. In addition, the mixing of silica fume increased the ε_{auto} of concrete containing fly ash, but it had a relatively insignificant effect on the ε_{auto} of concrete containing blast furnace slag. The ε_{auto} of a specimen using fly ash and blast furnace slag (0.28 FA20BFS25SF5) was the smallest among the values of the specimens with a W/B of 0.28, which is similar to the test result of the specimen with W/B 0.34.

Table 6 – The air content and workability of the fresh concretes.

	Mix	Slump (mm)	Air content (%)
W/B 0.40 & W/B 0.34	NPP-C	180	4.0
	0.34FA25	180	4.0
	0.34FA25BFS25	200	4.0
	0.34BFS50	200	4.8
	0.34BFS65SF5	180	3.6
		Slump flow-flow (mm)	
W/B 0.28	0.28FA25SF5	570	3.6
	0.28FA25BFS20SF5	500	4.5
	0.28BFS45SF5	560	4.6
	0.28BFS65SF5	590	3.5

NPP-C, nuclear power plant concrete; W/B, water-to-binder ratio.

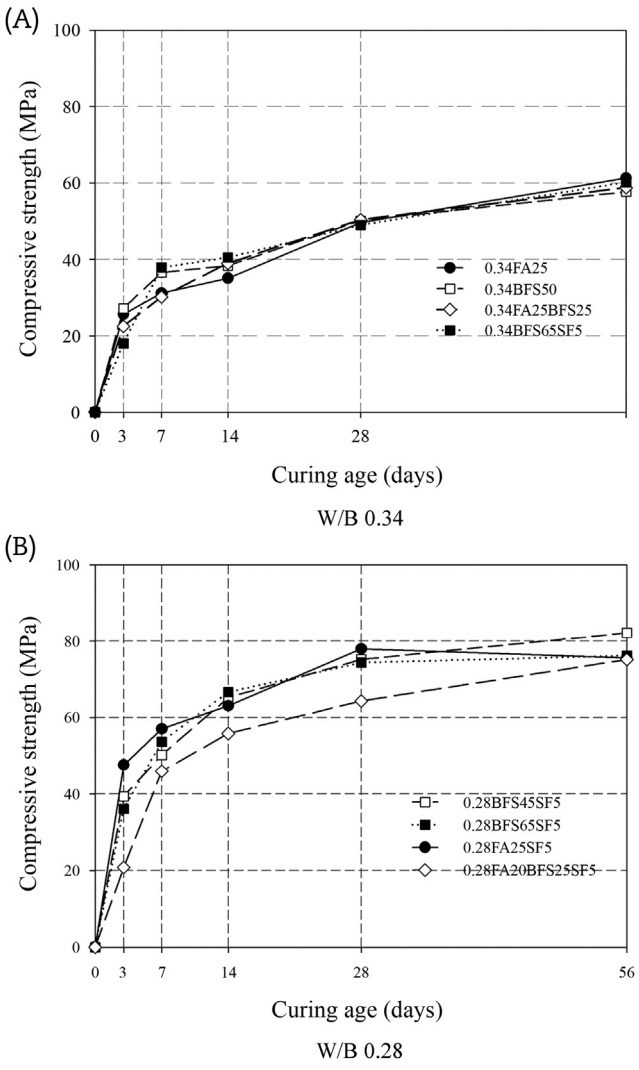

Fig. 4 – Compressive strength of the concretes versus the curing age.

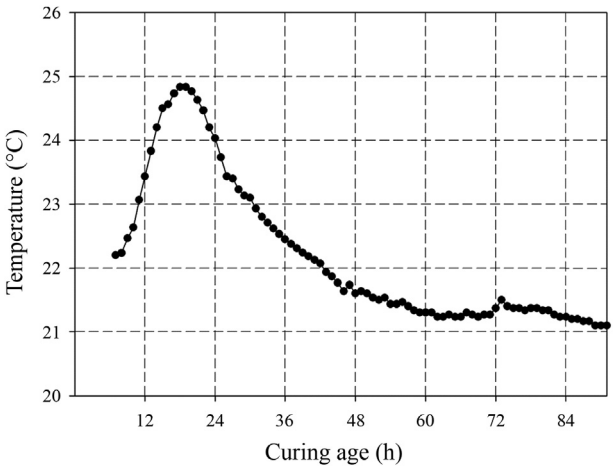

Fig. 5 – Internal temperature of the NPP-C specimen versus the curing age.

4.3. *The drying shrinkage of concrete*

Fig. 9 shows ε_{drying} of the concrete specimen and Fig. 10 shows the *NAS*.

The ε_{drying} of the NPP-C at a curing age of 91 days was 600.4 με. The ε_{drying} of the specimens with W/B 0.34 at 91 days were as follows (listed in decreasing order): 0.34BFS50 (688.9 με) > 0.34FA25 (666.2 με) > 0.34BFS65SF5 (560.5 με) > 0.34 FA25BFS25 (469.3 με).

The *NDS* of 0.34BFS50 showed a maximum value of 2.43 at 3 days, and it was 1.22–1.14 after a curing age of 28 days. The *NDS* of 0.34BFS50 at 3 days was largest among the *NDS*s of specimens with W/B 0.34. This finding may be because of the increase in the autogenous shrinkage from the mixing of blast furnace slag, as mentioned in Section 4.2. The *NDS* of 0.34BFS65SF5 had a maximum value of 1.69 at 4 days, and it was 0.99–0.93 after 28 days. The *NDS* of 0.34BFS65SF5 at 91 days decreased by 18.6%, compared to that of 0.34BFS50. The reason for this finding was the capillary pores decreased because of the pore filling effect of blast furnace slag and silica fume, which suppressed moisture evaporation [18].

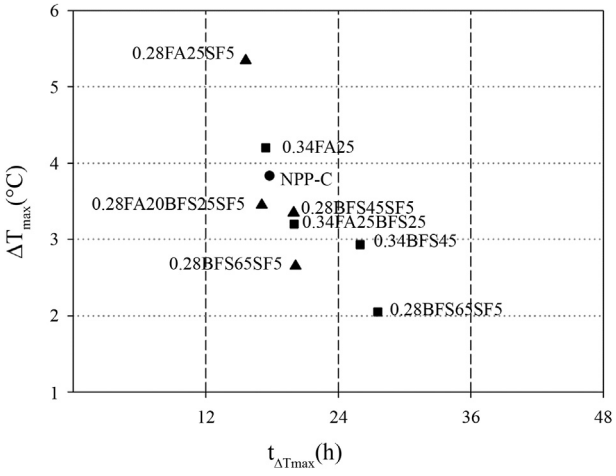

Fig. 6 – The ΔT_{max} of the NPP-HSC specimens.

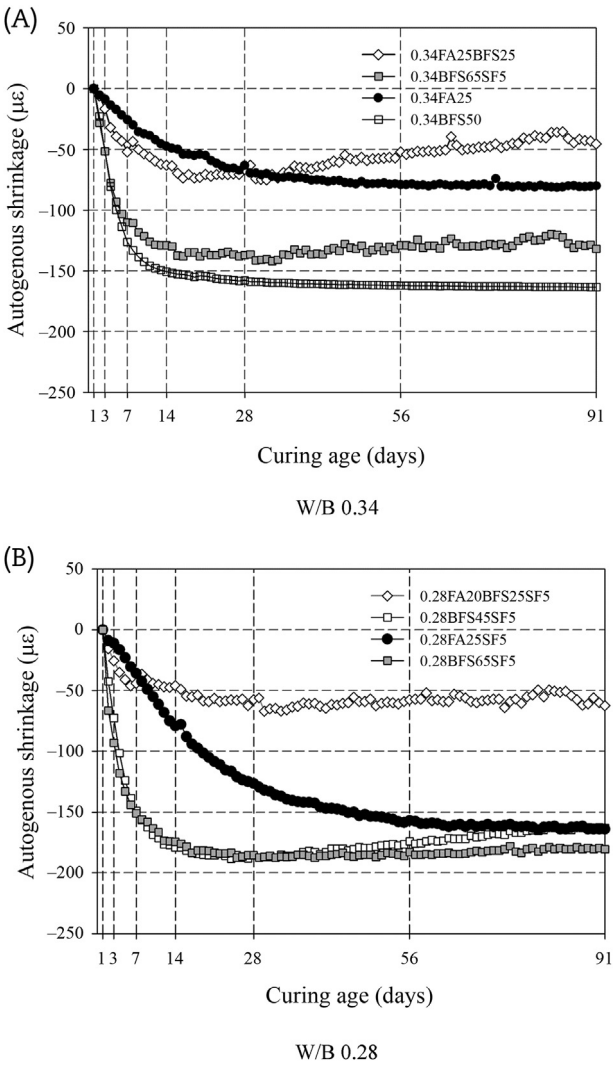

Fig. 7 – The autogenous shrinkage of NPP-HSCs versus the curing time.

The *NDS* of 0.34FA25 was < 1 until Day 3 because of the decrease in the autogenous shrinkage with incorporation of fly ash. The *NDS* of 0.34FA25 was 1.16–1.11 at the curing age of 3–91 days, and the *NDS* at a long-term curing age was similar to that of 0.34BFS50. The *NDS* of 0.34FA25BFS25 was < 1 over the entire curing age, and the *NDS* at 8–91 days was 0.85–0.77, which was the lowest value among the *NDS*s of specimens with W/B 0.34. The drying shrinkage of 0.34FA25BFS25 was not substantial, which may be because of the decrease in ε_{auto} from the mixing of fly ash and the moisture evaporation suppression effect of blast furnace slag. The ε_{drying} was smaller in specimens with W/B 0.28 than in specimens with W/B 0.34, regardless of the type of supplementary cementing materials; this finding may be because of the decrease in the amount of free water that could evaporate [19].

Fig. 11 shows the $\varepsilon_{auto}/\varepsilon_{drying}$ ratio of NPP-HSCs. In all mix proportions, the $\varepsilon_{auto}/\varepsilon_{drying}$ ratio had a relatively large value at an early curing age, and it decreased after 14 days. The $\varepsilon_{auto}/\varepsilon_{drying}$ shrinkage ratio increased with decreasing W/B and increased in the blast furnace slag substitution ratio. In particular, the $\varepsilon_{auto}/\varepsilon_{drying}$ ratio of 0.28BFS65SF5 was more than

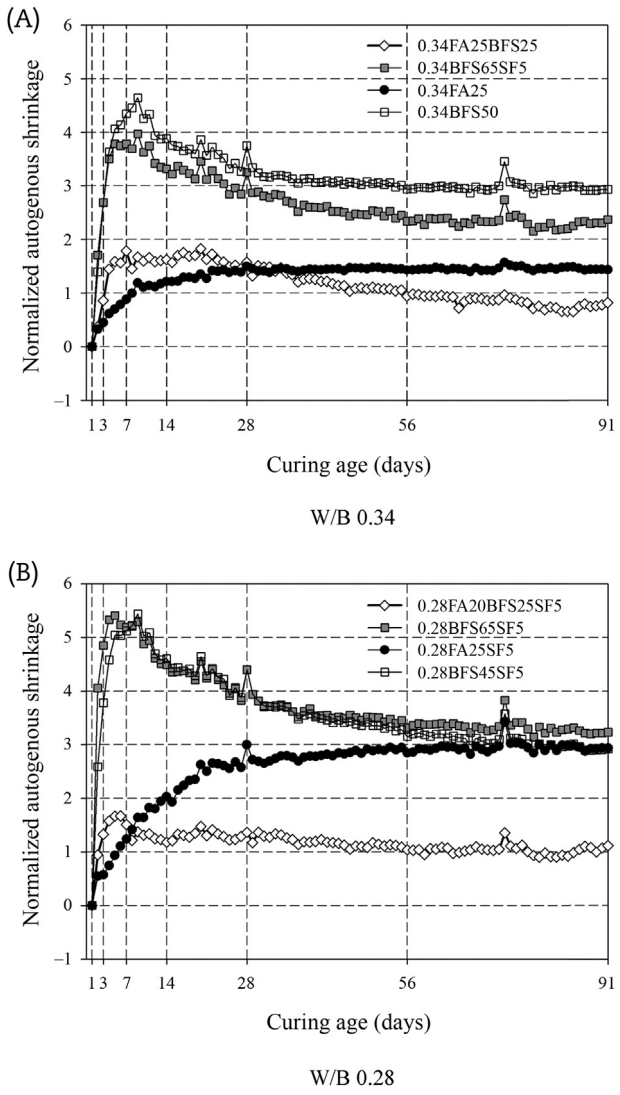

Fig. 8 – Normalized autogenous shrinkage. W/B, water-to-binder ratio.

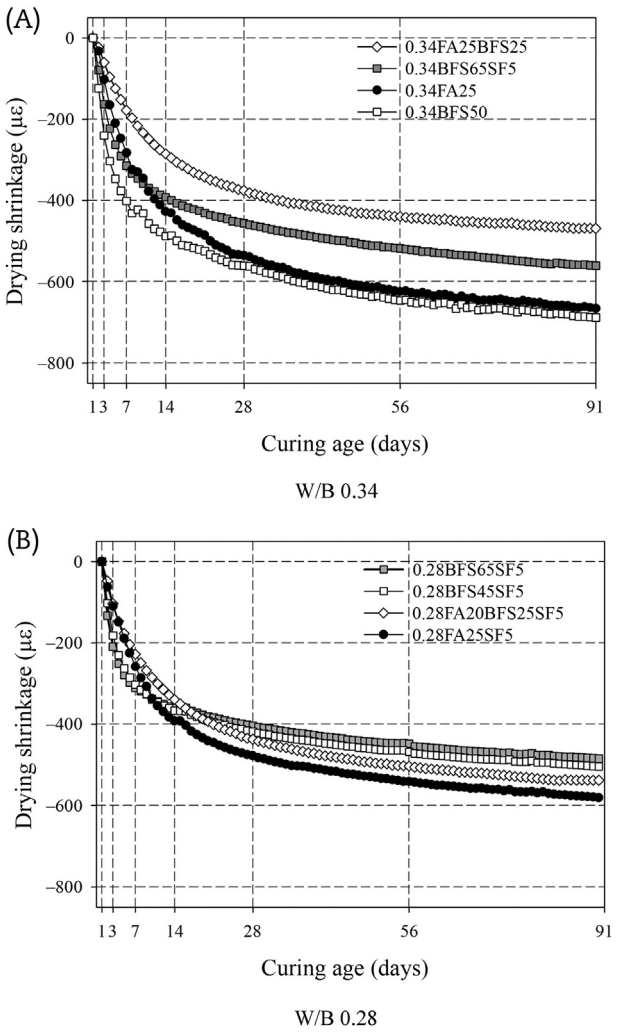

Fig. 9 – Drying shrinkage of NPP-HSCs versus the curing time. W/B, water-to-binder ratio.

40% until the curing age of 56 days. Therefore, to reduce the total shrinkage of NPP-HSC containing blast furnace slag, reducing the autogenous shrinkage by suppressing moisture loss at the early curing age would be effective.

4.4. *Restrained drying shrinkage and cracking of concrete (i.e., ring test)*

Fig. 12 shows the ε_s measured in ring specimens of NPP-HSC. The inner steel ring was compressed by the shrinkage of the concrete, but the compressive deformation decreased abruptly because of stress relaxation caused by cracking in the concrete. At the same curing age, the ε_s was generally higher in NPP-HSCs containing blast furnace slag than in NPP-HSCs containing fly ash, and the ε_s of NPP-HSCs increased with an increase in the mixing ratio of blast furnace slag.

Fig. 13 shows the t_{cr} and S of the NPP-HSCs. An inverse relationship between t_{cr} and S was evident. The equation of t_{cr} was obtained by regression analysis to evaluate the effect of S as follows:

$$t_{cr} = \exp\left(\frac{0.257 - S}{0.056}\right) > 0, \quad R^2 = 0.945 \tag{5}$$

The obtained equation indicates that S of NPP-HSCs should be lower than 0.088 MPa/d to obtain a t_{cr} value greater than that of existing NPP-C.

The S of NPP-HSCs with W/B 0.34 were as follows (listed in decreasing order): 0.34FA25 > 0.34FA25BFS25 > 0.34BFS50 > 0.34BFS65SF5; and all t_{cr} of the NPP-HSCs with W/B 0.34 were later than that of NPP-C. In particular, no cracking in 0.34BFS65SF5 occurred until the curing age of 91 days, and this reduced the S because of the low ε_{auto} and ε_{drying} of 0.34BFS65SF5 mentioned in Sections 4.2 and 4.3. The S of NPP-HSCs with W/B 0.28 were as follows (in decreasing order): 0.28FA25SF5 > 0.28BFS65SF5 > 0.28BFS45SF5 > 0.28 FA20BFS25SF5. The cracking of 0.28FA25SF5 appeared significantly earlier than that of NPP-C. It appears that silica fume, even at a 5% ratio, seriously affected the increase of the S, resulting in 0.28FA25SF5 cracking earlier. The ε_{auto} and ε_{drying} of 0.28BFS45SF5 and 0.28BFS65SF5 were not significantly different. However, the S of 0.28BFS65SF5

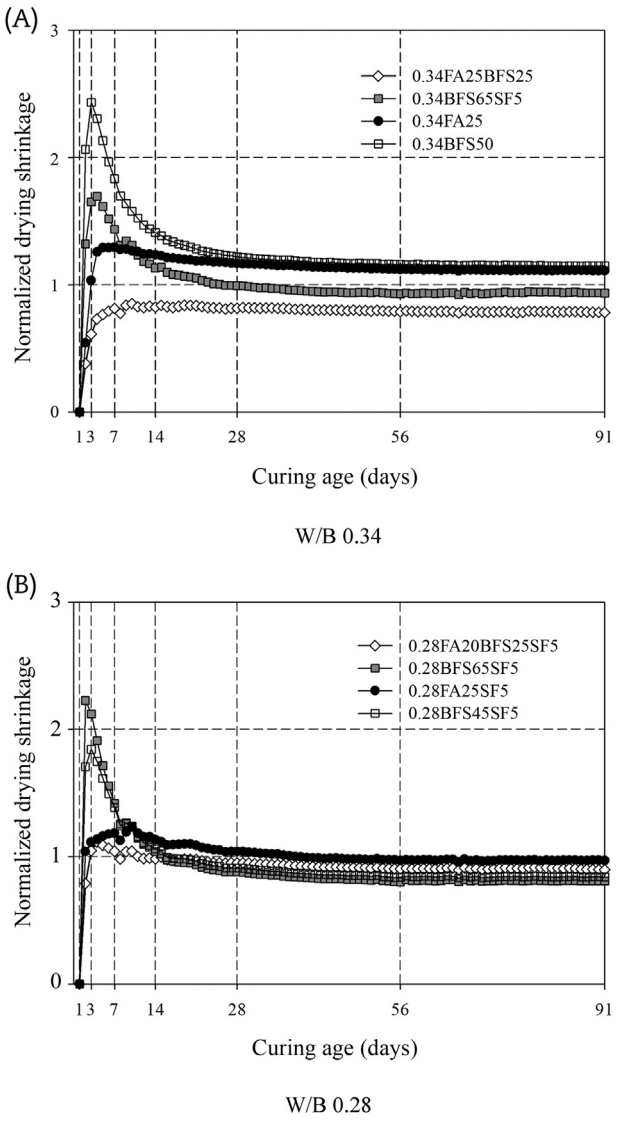

Fig. 10 – Normalized drying shrinkage. W/B, water-to-binder ratio.

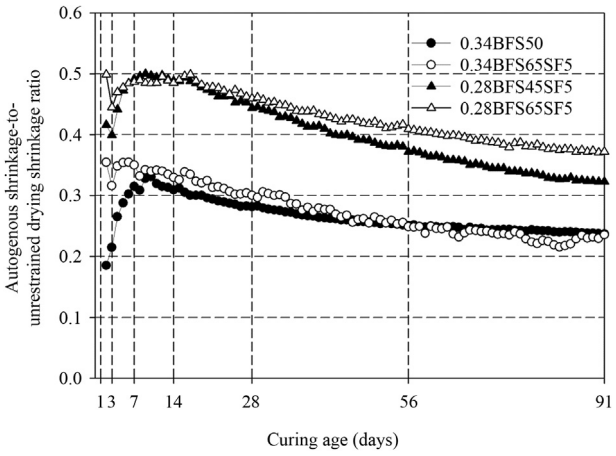

Fig. 11 – Autogenous shrinkage/unrestrained drying shrinkage ratio.

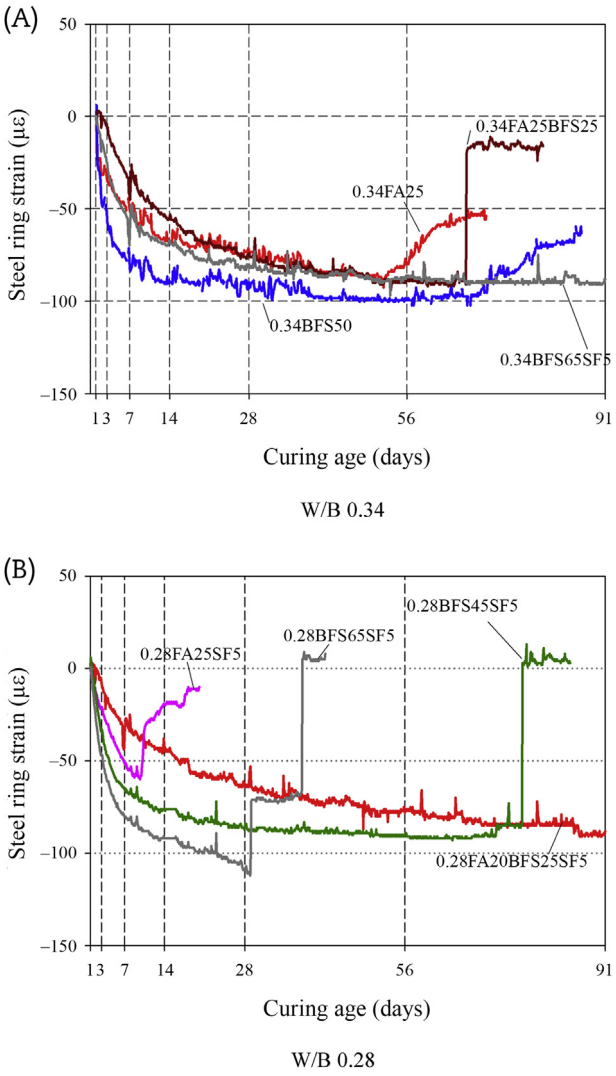

Fig. 12 – Steel ring strain of NPP-HSCs. NPP-HSC, nuclear power plant high strength concrete; W/B, water-to-binder ratio.

was larger than that of 0.28BFS45SF5, resulting in the earlier cracking of 0.28BFS65SF5. This indicated that the NPP-HSCs could be more vulnerable to shrinkage cracking due to the increased degree of restraint from the mixing of a large amount of blast furnace slag.

5. Conclusion

This study reported the shrinkage characteristics and cracking potentials of NPP-HSCs under review for the application in the construction of NPPs. The following can be concluded, based on information in the results and discussion of autogenous shrinkage, drying shrinkage, and restrained shrinkage of the NPP-HSCs:

(1) The ε_{auto} and ε_{drying} of NPP-HSCs containing blast furnace slag were the greatest among those of NPP-HSCs at an

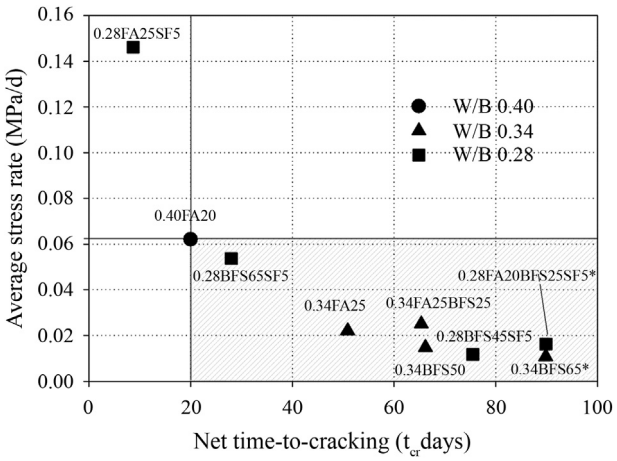

Fig. 13 – The t_{cr} and S of NPP-HSCs. W/B, water-to-binder ratio.

early age. In particular, ε_{auto} at 5 days and ε_{drying} at 3 days of 0.28BFS65SF5 were up to 5.40 times greater and 2.43 times greater, respectively, than those of existing NPP-C. Thus, NPP-HSCs containing blast furnace slag had the risk of early age shrinkage cracking. Therefore, the application of proper curing methods are essential to reduce the ε_{auto} and ε_{drying} of NPP-HSCs containing blast furnace slag at an early age.

(2) There is an inverse relationship between S and t_{cr} of the NPP-HSCs ($t_{cr} = \exp((0.257 - S)/0.056) > 0$, $R^2 = 0.945$). This finding indicated that the S of NPP-HSCs should be lower than 0.088 MPa/day to obtain a t_{cr} value greater than that of existing NPP-C.

(3) The ε_{auto} and ε_{drying} of NPP-HSCs containing blast furnace slag were 3.75–4.28 times higher and 1.02–1.66 times higher, respectively, than those of NPP-C at t_{cr}; however, all S values of NPP-HSCs containing blast furnace slag were 12.7–83.4% lower than that of the existing NPP-C. Blast furnace slag content in the range of 50–65% of the binder did not significantly affect the S values of NPP-HSCs with W/B 0.34. However, with an increase of blast furnace slag content from 45–65% of the binder at W/B 0.28, the S values of NPP-HSCs increased 4.6 times, despite the 18% reduction of their ε_{drying} value. Therefore, for NPP-HSCs with less than W/B 0.28, the application of blast furnace slag content with 65% of a binder should be considered with caution.

(4) The ε_{drying} of NPP-HSC containing fly ash were lower than NPP-HSC containing blast furnace slag for the first 7 days. However, after 7 days, the ε_{drying} of the NPP-HSCs containing fly ash increased significantly, thereby resulting in a higher S than those of the NPP-HSCs containing blast furnace slag. In particular, for the mix of 0.28FA25SF5, using silica fume, even at a 5% ratio, and reducing W/B from 0.34 to 0.28 increased the S as much as 6.67 times with respect to that of 0.34FA25. Therefore, the use of fly ash in conjunction with silica fume should be restricted for the NPP-HSCs with a compressive strength greater than 10,000 psi.

(5) For a given W/B, NPP-HSCs containing both fly ash and blast furnace slag gave the smallest ε_{auto} among the NPP-HSCs, and their S values decreased 59.8–73.9%, compared to that of the NPP-C. Thus, for reducing the cracking potential of NPP-HSC, fly ash used in conjunction with blast furnace slag is recommended over the use of a single by-product, fly ash only, or blast furnace slag only.

(6) The cracking of all mix proportions, with exception of 0.28FA25SF5, appeared later than in NPP-C, which suggested that the durability of a NPP against shrinkage cracking could be improved by applying any of the seven mix proportions used in this study.

The results in this paper demonstrated that by-products can be used as supplementary cementing materials of NPP-HSC to improve the design life and safety of NPPs. However, in this study, the shrinkage characteristics and cracking potentials of NPP-HSCs were evaluated only under standard curing conditions; thus, to apply the NPP-HSCs to the construction of NPPs in foreign countries, further research that investigates various curing conditions is necessary.

Conflicts of interest

All authors declare no conflicts of interest.

Acknowledgments

This research was supported by the Nuclear Power R&D Program of the Korea Institute of Energy Technology Evaluation and Planning (Seoul, Korea), by a grant funded by the Korea Government Ministry of Knowledge Economy (Grant No., 2011T100200161), and by the Basic Science Research Program through the National Research Foundation of Korea (NRF) funded by the Ministry of Education, Science and Technology (Sejong, Korea; Grant No., NRF-2013R1A1A2012788). In addition, this study was supported in part by a grant from the Korea University (Seoul, Korea).

REFERENCES

[1] P.K. Mehta, High-performance, High-volume Fly Ash Concrete for Sustainable Development, Proceedings of the International Workshop on Sustainable Development and Concrete Technology, Iowa State University, Ames, IA, 2004, pp. 3–14.

[2] D. Allopi, S. Zulu, Influence of high content fly ash on concrete durability, International Journal of Engineering and Innovative Technology 3 (2014) 150–155.

[3] K.G. Babu, V.S.R. Kumar, Efficiency of GGBS in concrete, Cement and Concrete Research 30 (2000) 1031–1036.

[4] S.A. Khedr, M.N. Abou-Zeid, Characteristics of silica-fume concrete, Journal of Materials in Civil Engineering 6 (1994) 357–375.

[5] P. Chindaprasirt, S. Homwuttiwong, V. Sirivivatnanon, Influence of fly ash fineness on strength, drying shrinkage and sulfate resistance of blended cement mortar, Cement and Concrete Research 34 (2004) 1087–1092.

[6] P.K. Mehta, Durability of Concrete in Marine Environment—A Review Vol. 65, ACI Special Publication. American Concrete Institute, Farmington Hills, MI, 1980, pp. 1–20.
[7] W. Chan, C. Wu, Durability of concrete with high cement replacement, Cement and Concrete Research 30 (2000) 865–879.
[8] J.M. Noh, K.J. Kwon, H.S. Nah, W.S. Joung, Practical experimental study on multi-component self-compacting concrete, Journal of the Korea Concrete Institute 16 (2004) 760–763.
[9] J.E. Kim, W.S. Park, S.H. Yun, D.G. Kim, J.M. Noh, Development of high performance concrete containing admixture in nuclear power plants, Applied Mechanics and Materials 357 (2013) 1062–1065.
[10] P.C. Aitcin, A. Neville, P. Acker, Integrated view of shrinkage deformation, Concrete International 19 (1997) 35–41.
[11] A.B. Hossain, J. Weiss, Assessing residual stress development and stress relaxation in restrained concrete ring specimens, Cement and Concrete Composites 26 (2004) 531–540.
[12] H.T. See, E.K. Attiogbe, M.A. Miltenberger, Shrinkage cracking characteristics of concrete using ring specimens, Materials Journal 100 (2003) 239–245.
[13] K. Tang, S. Millard, G. Beattie, Early-age heat development in GGBS concrete structures, Proceedings of the Institution of Civil Engineers–Structures and Buildings 168 (2015) 541–553.
[14] E.H. Kadri, R. Duval, Hydration heat kinetics of concrete with silica fume, Construction and Building Materials 23 (2009) 3388–3392.
[15] K. Lee, H. Lee, S. Lee, G. Kim, Autogenous shrinkage of concrete containing granulated blast-furnace slag, Cement and Concrete Research 36 (2006) 1279–1285.
[16] S. Lim, T. Wee, Autogenous shrinkage of ground-granulated blast-furnace slag concrete, Materials Journal 97 (2009) 587–593.
[17] M. Zhang, C. Tam, M. Leow, Effect of water-to-cementitious materials ratio and silica fume on the autogenous shrinkage of concrete, Cement and Concrete Research 33 (2003) 1687–1694.
[18] J. Li, Y. Yao, A study on creep and drying shrinkage of high performance concrete,, Cement and Concrete Research 31 (2001) 1203–1206.
[19] P. Nath, P.K. Sarker, Properties of high strength concrete containing class F fly ash, in: P.K. Sarker (Ed.), Fly Ash: Sources, Applications and Potential Environmental Impacts, Nova Science Publications Inc., New York (NY), 2014, pp. 195–226.
[20] ASTM Standard C143/C143M, 2012, Slump of Hydraulic-Cement Concrete, ASTM International, West Conshohocken, PA, 2012.
[21] ASTM Standard C173/C173M, 2014, Air Content of Freshly Mixed Concrete by the Volumetric Method, ASTM International, West Conshohocken, PA, 2014.
[22] ASTM Standard C39/C39M, 2015, Compressive Strength of Cylindrical Concrete Specimens, ASTM International, West Conshohocken, PA, 2015.
[23] KS F 2586, 2010, Autogenous shrinkage and expansion of cement paste, mortar and concrete, Korean Standards Association, Seoul, 2010.
[24] ASTM C596, 2009, Drying Shrinkage of Mortar Containing Hydraulic Cement, ASTM International, West Conshohocken, PA, 2009.
[25] American Association of State Highway and Transport Officials (AASHTO) PP 34-99, Standard Practice for Estimating the Crack Tendency of concrete, 2005. Washington, D. C.